Deep geomagnetic sounding by Sq variations: A 3-D inversion based on the regional-to-local transfer functions

Libor Šachl, Jakub Velímský

12.10. 2022

Current section

1 Introduction
2 Forward modelling
3 Inverse modelling
4 Synthetic tests
5 3-D inversion of real data

What is our aim?

- electric conductivity of upper-mantle using Sq variations
- recall:
  - Syntetická 3D inverze magnetického pole oceánských slapů
    - adjoint approach
    - source
    - region
    - data
  - 3-D modelování EM indukce s ionosférickými zdroji: Slepiány a lokálně-regionální přenosové funkce

Regional to local transfer functions

- analysis within 5-day (3-day) segments
  - index Kp
  - rate of change $\frac{\mathrm{d}\,\mathrm{Dst}}{\mathrm{d}t}$
- interpolate horizontal field using slepians (regional)
- use Z component (local) to derive the transfer function (TF)
- $\Rightarrow$ model of external field is not needed

Current section

1 Introduction

2 Forward modelling

3 Inverse modelling

4 Synthetic tests

5 3-D inversion of real data

Governing equations

Electro-magnetic induction (EMI) equation in the frequency domain

$$\nabla \times [\rho(\boldsymbol{r}) \nabla \times \boldsymbol{B}(\boldsymbol{r}; \omega)] - i\omega\mu_0 \boldsymbol{B}(\boldsymbol{r}; \omega) = 0,$$
$$\nabla \cdot \boldsymbol{B}(\boldsymbol{r}; \omega) = 0,$$

with boundary conditions at the Earth's surface

$$B^0_{jm}(a; \omega) = 0,$$
$$B^{+1}_{jm}(a; \omega) = \int_{\Omega} \boldsymbol{g}_{\alpha}(\Omega) \cdot \overline{\boldsymbol{S}}^{(+1)}_{jm}(\Omega) \mathrm{d}\Omega.$$

Slepians

- horizontal poloidal SH vector functions (bandwidth limited)

$$\boldsymbol{g}_\alpha(\Omega) = \sum_{j=1}^{j^{\mathrm{s}}_{\max}} \sum_{m=-j}^{j} g^{\alpha}_{jm} \boldsymbol{s}^{(+1)}_{jm}(\Omega),$$

  $\alpha = 1, \ldots, N_{\mathrm{s}} \leq j^{\mathrm{s}}_{\max}(j^{\mathrm{s}}_{\max} + 2)$

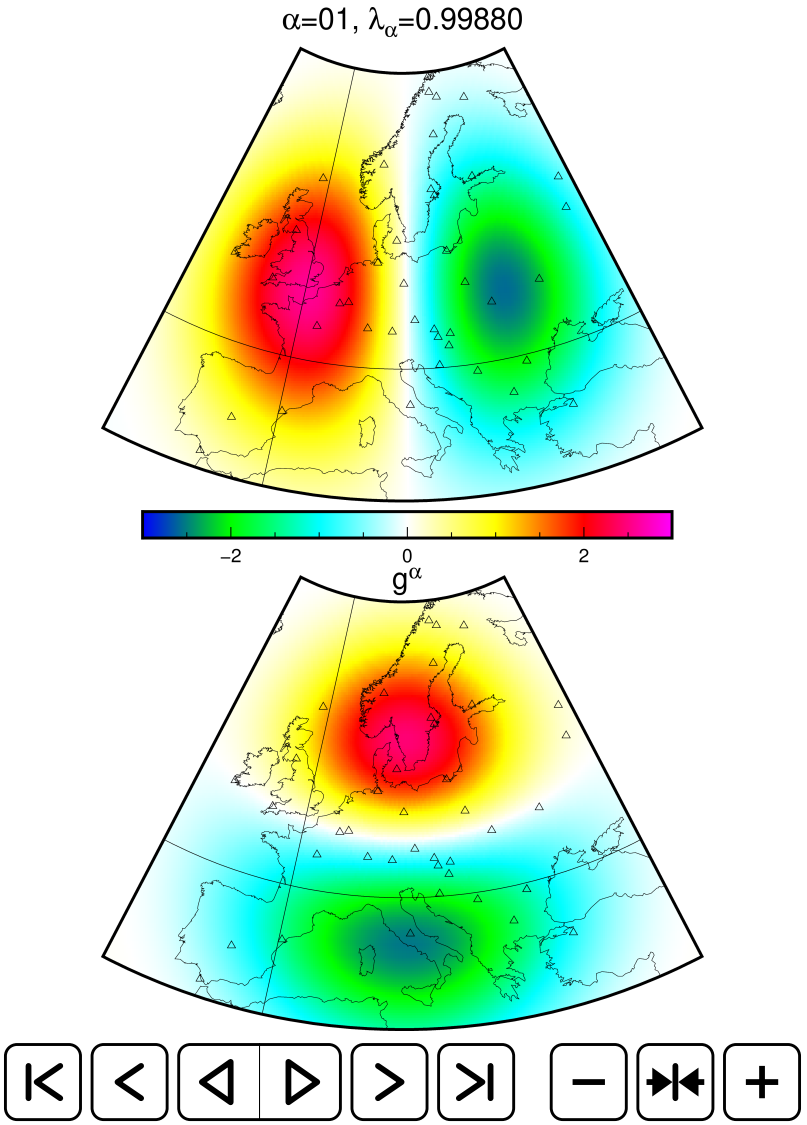
- orthogonal families of functions defined on a common domain $R \subset \Omega$

$$\int_R \boldsymbol{g}_\alpha(\Omega) \cdot \boldsymbol{g}_\beta(\Omega) \mathrm{d}\Omega = \lambda_\alpha \delta_{\alpha\beta}$$

- optimally concentrated in the domain

$$\lambda_\alpha = \frac{\int_R \boldsymbol{g}_\alpha(\Omega) \cdot \boldsymbol{g}_\alpha(\Omega) \mathrm{d}\Omega}{\int_\Omega \boldsymbol{g}_\alpha(\Omega) \cdot \boldsymbol{g}_\alpha(\Omega) \mathrm{d}\Omega} = \max,$$

Slepians over Europe for $j^{\mathrm{S}}_{\mathrm{max}} = 20$



ElmgFD

- weak formulation of the EMI equation
- piecewise-linear 1-D finite elements in radial coordinate
- complex vector spherical harmonic functions in angular coordinates
- parallelized using OpenMP

Current section

1 Introduction

2 Forward modelling

3 Inverse modelling

4 Synthetic tests

5 3-D inversion of real data

Model space

$$\log_{10} \frac{\sigma(\mathbf{m}, \mathbf{m}_0; \boldsymbol{r})}{\sigma_0} = \sum_{\beta=1}^{M} m_\beta \xi_\beta(\boldsymbol{r}) + \sum_{\beta=M+1}^{M+M_0} m_{0\beta} \xi_\beta(\boldsymbol{r})$$

- $\mathbf{m} \in \mathbb{R}^M$ and $\mathbf{m}_0 \in \mathbb{R}^{M_0}$
- $\xi_\beta(\boldsymbol{r})$, $\beta = 1, 2, \ldots, M + M_0$ are piecewise constant functions,

$$\begin{aligned} \xi_\beta(\boldsymbol{r}) &= \begin{cases} 1 & \boldsymbol{r} \in I_\beta \\ 0 & \boldsymbol{r} \notin I_\beta \end{cases}, \\ I_\beta \cap I_{\beta'} &= \emptyset \quad \text{for } \beta \neq \beta', \\ \bigcup_{\beta=1}^{M+M_0} I_\beta &= G. \end{aligned}$$

Penalty function

Consider N_p periods, N_s slepians and N_o observatories $\Rightarrow$

$$\widetilde{\mathbf{m}}(\lambda) = \arg \min_{\mathbf{m} \in R^M} \left[\chi^2(\mathbf{m}) + \lambda R^2(\mathbf{m}) \right]$$

$$\chi^2(\mathbf{m}) = \frac{1}{2\, N_\mathrm{p} N_\mathrm{s} N_\mathrm{o}} \sum_{p=1}^{N_\mathrm{p}} \sum_{\alpha=1}^{N_\mathrm{s}} \sum_{k=1}^{N_\mathrm{o}} w_{k\alpha}^{p} \left| T_{k\alpha}^{p} - T_{k\alpha}^{p,\mathrm{obs}} \right|^2 ,$$

$$R^2(\mathbf{m}) = \frac{1}{a} \int_G \left| \nabla_\mathrm{h} \log_{10} \sigma(\mathbf{m}; \boldsymbol{r}) \right|^2 \mathrm{d}V .$$

How to find $\widetilde{\mathbf{m}}$ numerically?

Limited-memory quasi-Newton minimization approach with the Broyden-Fletcher-Goldfarb-Shanno formula (Press et al., 1992, Section 10.7) used for gradual updates of the approximate inverse of the Hessian

$$\Downarrow$$

M-dimensional gradient $\mathbf{D_m}\chi^2(\mathbf{m})$ is needed,

$$\mathbf{D_m}\chi^2(\mathbf{m}) = \left(\mathrm{D}_1\chi^2(\mathbf{m}), \mathrm{D}_2\chi^2(\mathbf{m}), \ldots, \mathrm{D}_M\chi^2(\mathbf{m})\right),$$

where

$$\mathrm{D}_\beta\chi^2 = \frac{\partial\chi^2}{\partial m_\beta}$$

Adjoint approach

According to Šachl et al. (2022) and Maksimov and Velímský (2017), we solve one forward and one adjoint problem for each period ω_p and each Slepian function $\boldsymbol{g}_\alpha(\Omega)$.

Forward problem:

$$\nabla \times [\rho(\boldsymbol{r}) \nabla \times \boldsymbol{B}_\alpha(\boldsymbol{r}; \omega_p)] - \mathrm{i}\omega_p \mu_0 \boldsymbol{B}_\alpha(\boldsymbol{r}; \omega_p) = \boldsymbol{0},$$
$$\nabla \cdot \boldsymbol{B}_\alpha(\boldsymbol{r}; \omega_p) = 0,$$

with BC at the Earth's surface

$$B^{(0)}_{jm,\alpha}(a; \omega_p) = 0,$$
$$B^{(+1)}_{jm,\alpha}(a; \omega_p) = \int_\Omega \boldsymbol{g}_\alpha(\Omega) \cdot \overline{\boldsymbol{S}}^{(+1)}_{jm}(\Omega) \mathrm{d}\Omega.$$

Adjoint approach

Adjoint problem:

$$\nabla \times \left[\rho(\boldsymbol{r})\,\nabla \times \hat{\boldsymbol{B}}_\alpha(\boldsymbol{r};\omega_p)\right] + \mathrm{i}\omega_p\mu_0\hat{\boldsymbol{B}}_\alpha(\boldsymbol{r};\omega_p) = \boldsymbol{0}$$

or

$$\nabla \times \left[\rho(\boldsymbol{r})\,\nabla \times \overline{\hat{\boldsymbol{B}}}_\alpha(\boldsymbol{r};\omega_p)\right] - \mathrm{i}\omega_p\mu_0\overline{\hat{\boldsymbol{B}}}_\alpha(\boldsymbol{r};\omega_p) = \boldsymbol{0}$$

with BC at the Earth's surface

$$\overline{\hat{B}}^{(0)}_{jm,\alpha}(a;\omega_p) = 0,$$

$$\overline{\hat{B}}^{(+1)}_{jm,\alpha}(a;\omega_p) = \frac{2\pi\mathrm{i}}{N}\sum_k w^p_{k\alpha}\left(\overline{T}^p_{k\alpha} - \overline{T}^{p,\mathrm{obs}}_{k\alpha}\right) Y_{jm}(\Omega_k)$$

Adjoint approach

Derivative of misfit with respect to m_β:

$$\mathrm{D}_\beta \chi^2(\mathbf{m}) = \frac{2}{4\pi\, a^3\, \mu_0} \mathrm{Re} \left(\int_G \mathrm{D}_\beta \rho(\mathbf{m}; \boldsymbol{r}) I \, \mathrm{d}V \right),$$

where

$$D_\beta \rho = -(\ln 10) \rho(\mathbf{m}; \boldsymbol{r}) \zeta_\beta(\boldsymbol{r})$$

and

$$I = \sum_{p=1}^{N_\mathrm{p}} \sum_{\alpha=1}^{N_s} \frac{1}{\omega_p} \nabla \times \boldsymbol{B}_\alpha(\mathbf{m}; \boldsymbol{r}; \omega_p) \cdot \nabla \times \hat{\overline{\boldsymbol{B}}}_\alpha(\mathbf{m}; \boldsymbol{r}; \omega_p).$$

Current section

1 Introduction

2 Forward modelling

3 Inverse modelling

4 Synthetic tests

5 3-D inversion of real data

General idea

1. Forward modelling: conductivity model + EM forcing $\rightarrow$ TF functions
2. Inverse modelling: TF functions $\rightarrow$ recovered conductivity model

Earth conductivity model

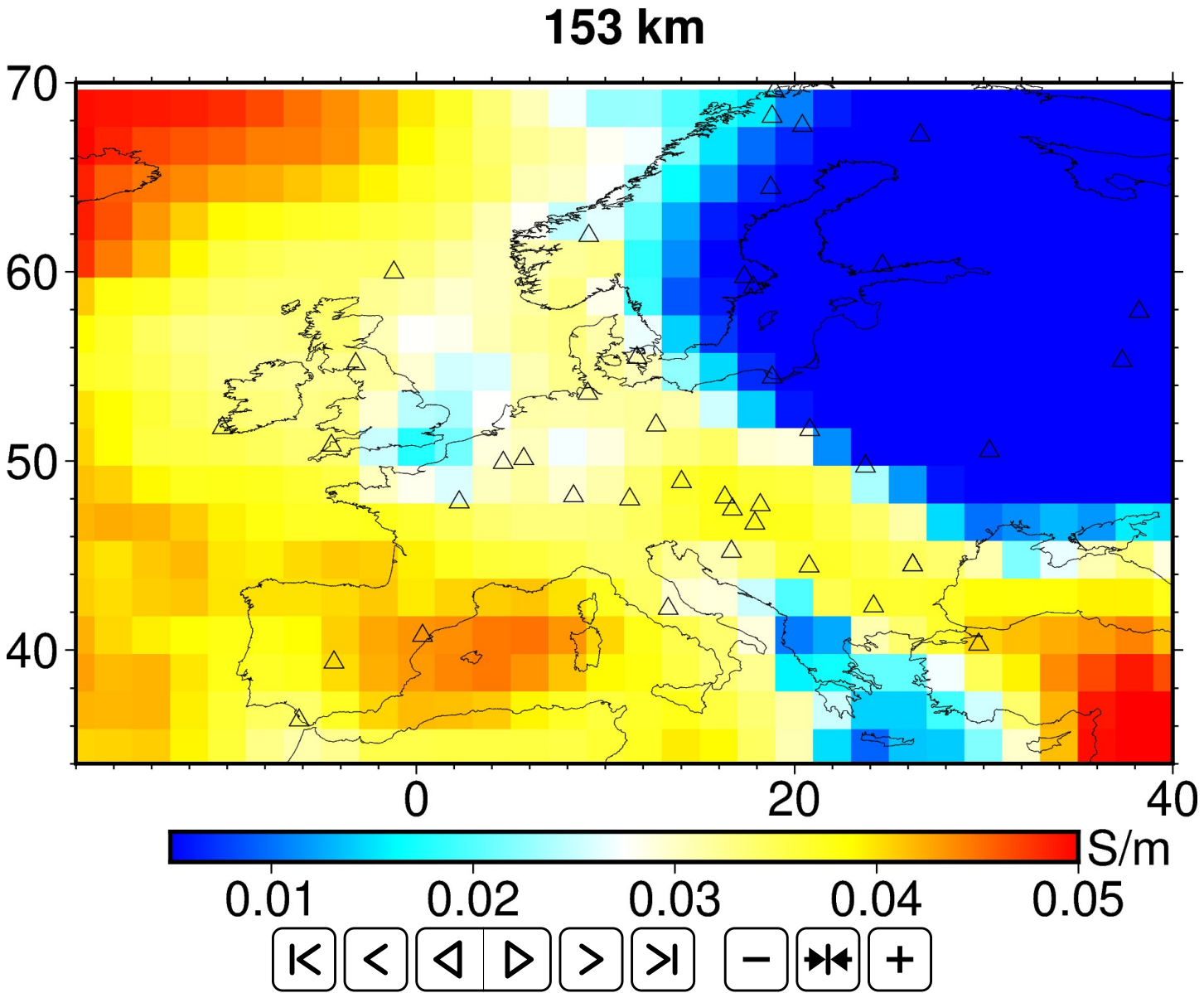
- litosphere (upper aprox. 20 km)
  - oceans: 3-D σ_{oc} of Tyler et al. (2017), $\langle \sigma_{oc} \rangle = 3.31 \pm 0.23$ S/m
  - sediments: 3-D σ_{sed} of Everett et al. (2003) (Grayver (2021)?)
- upper mantle: 1-D + 3-D WINTERC-e model
- lower mantle: 1-D profile of Grayver et al. (2017)
- core: $\sigma_{core} = 2 \times 10^5$ S/m

3-D conductivity model WINTERC-e

Original model (Martinec et al., 2021):

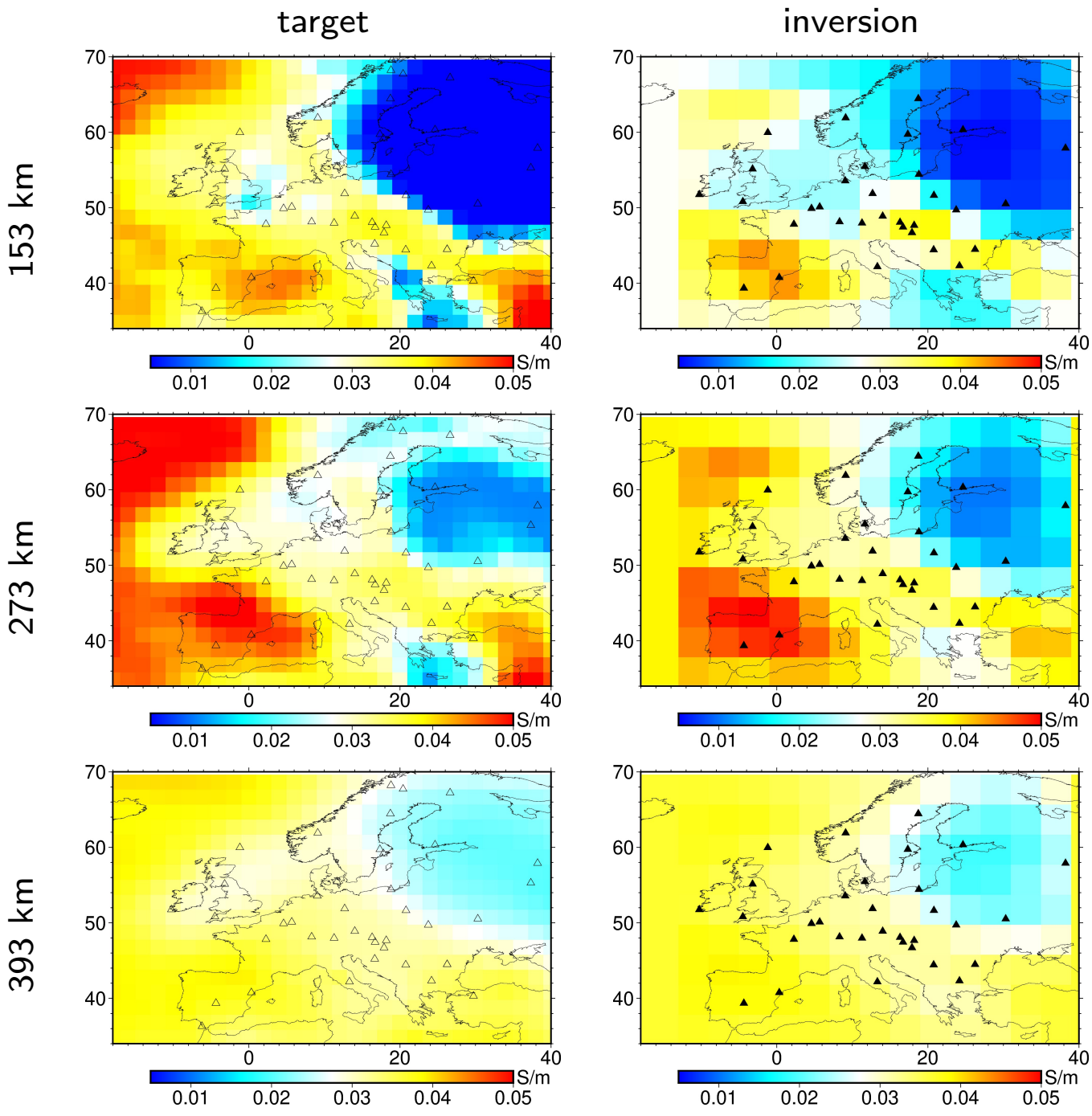
- created using no EM data!
  - seismic waveform tomography, global satellite gravity, surface elevation, heat flow data $\rightarrow$ WINTERC-G (Fullea et al., 2021)
  - WINTERC-G + conductivity measurements $\rightarrow$ WINTERC-e
- upper-mantle model: 0-402 km
- two end-members
  - Wd-emin: dry, no melt
  - Wd-emax: 140 ppm of water, melting

Model Wd-emax



EImgFD configuration

- spherical-harmonic truncation degree $j_{max} = 60$
- total of 204 layers
  - 3-D ocean: 141
  - 1-D upper-mantle: 7
  - 3-D upper-mantle: 13
  - 1-D core and lower-mantle: 43
- inverse problem
  - $4^\circ \times 4^\circ$ grid cells
  - 13 layers
  - 1521 model parameters


target
inversion
153 km
273 km
393 km
70
60
50
40
0
20
40
S/m
0.01
0.02
0.03
0.04
0.05

Quality assessment

In each layer, we calculate Pearson's correlation coefficient C_r,

$$C_r(\sigma, \sigma_T, r) = \frac{\int\limits_R \log_{10}\left[\sigma(\boldsymbol{r})/\overline{\sigma}(r)\right] \log_{10}\left[\sigma_T(\boldsymbol{r})/\overline{\sigma_T}(r)\right] d\Omega}{\sqrt{\left\{\int\limits_R \log_{10}^2\left[\sigma(\boldsymbol{r})/\overline{\sigma}(r)\right] d\Omega\right\}\left\{\int\limits_R \log_{10}^2\left[\sigma_T(\boldsymbol{r})/\overline{\sigma_T}(r)\right] d\Omega\right\}}},$$

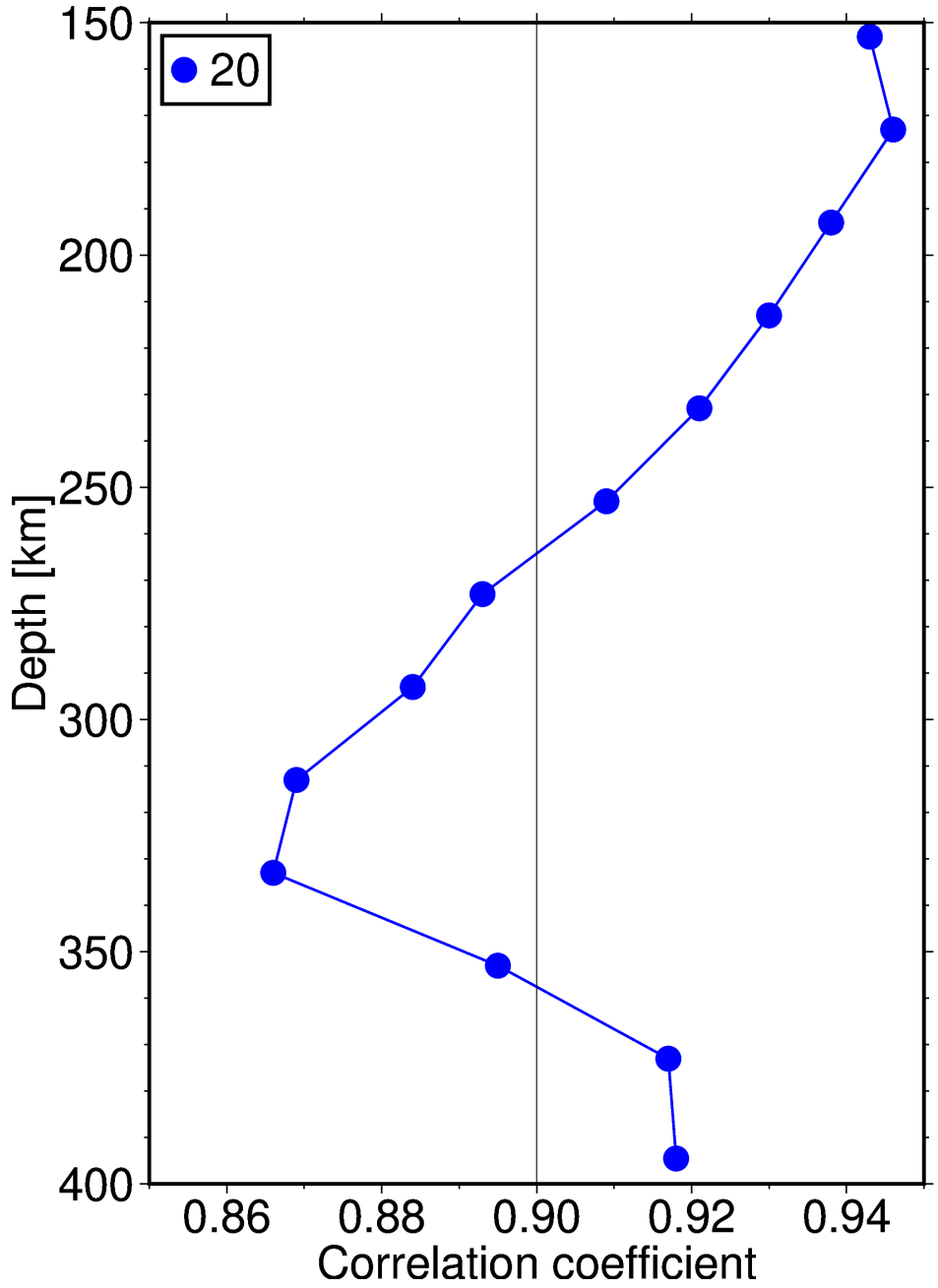


Figure: Depth profiles of correlation coefficients for $T = 24$ h using $j^{\mathrm{s}}_{\mathrm{max}} = 20$ and $N_s = 20$.

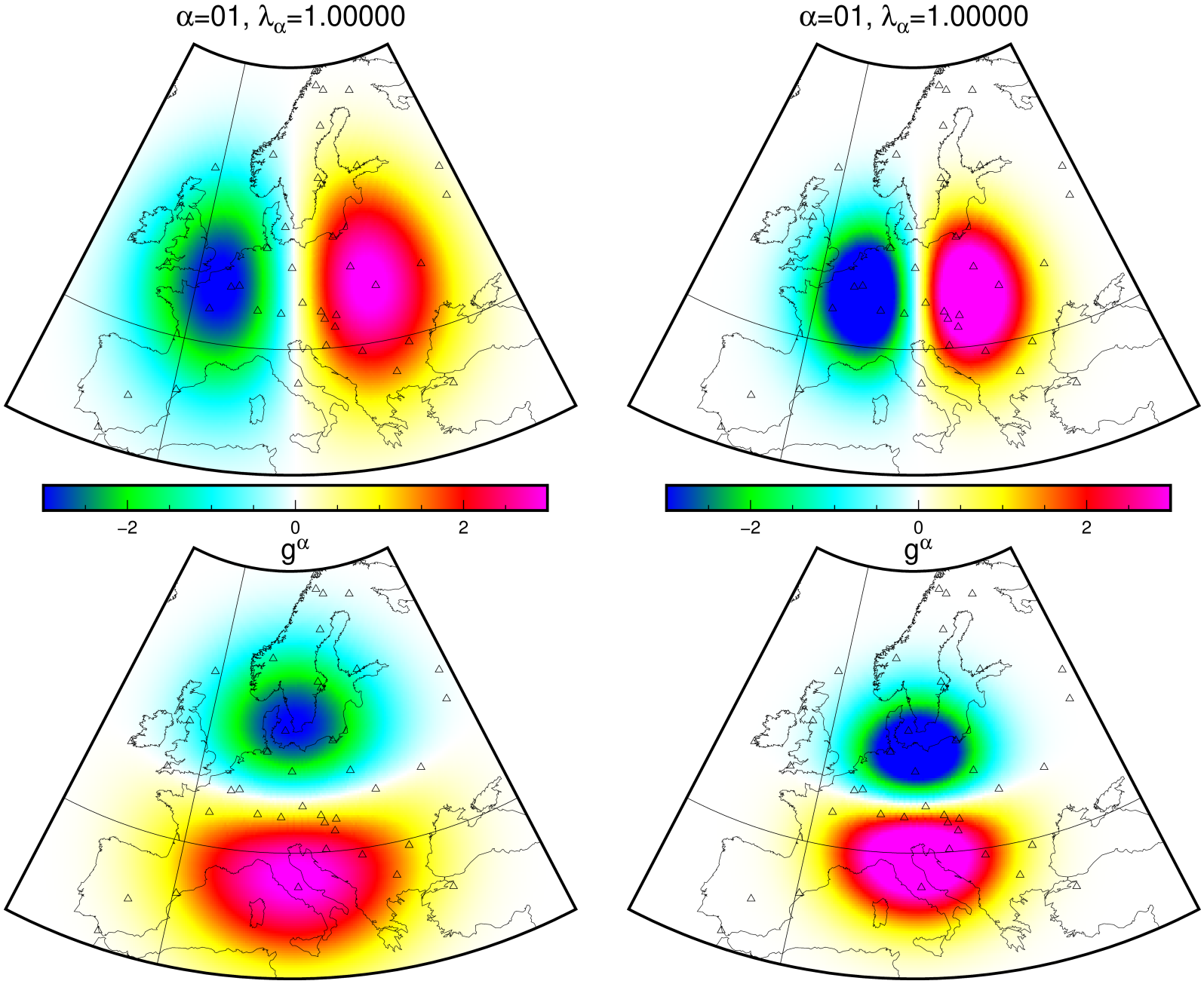


Figure: First slepian for $j^{\mathrm{s}}_{\max} = 30$ and 60.

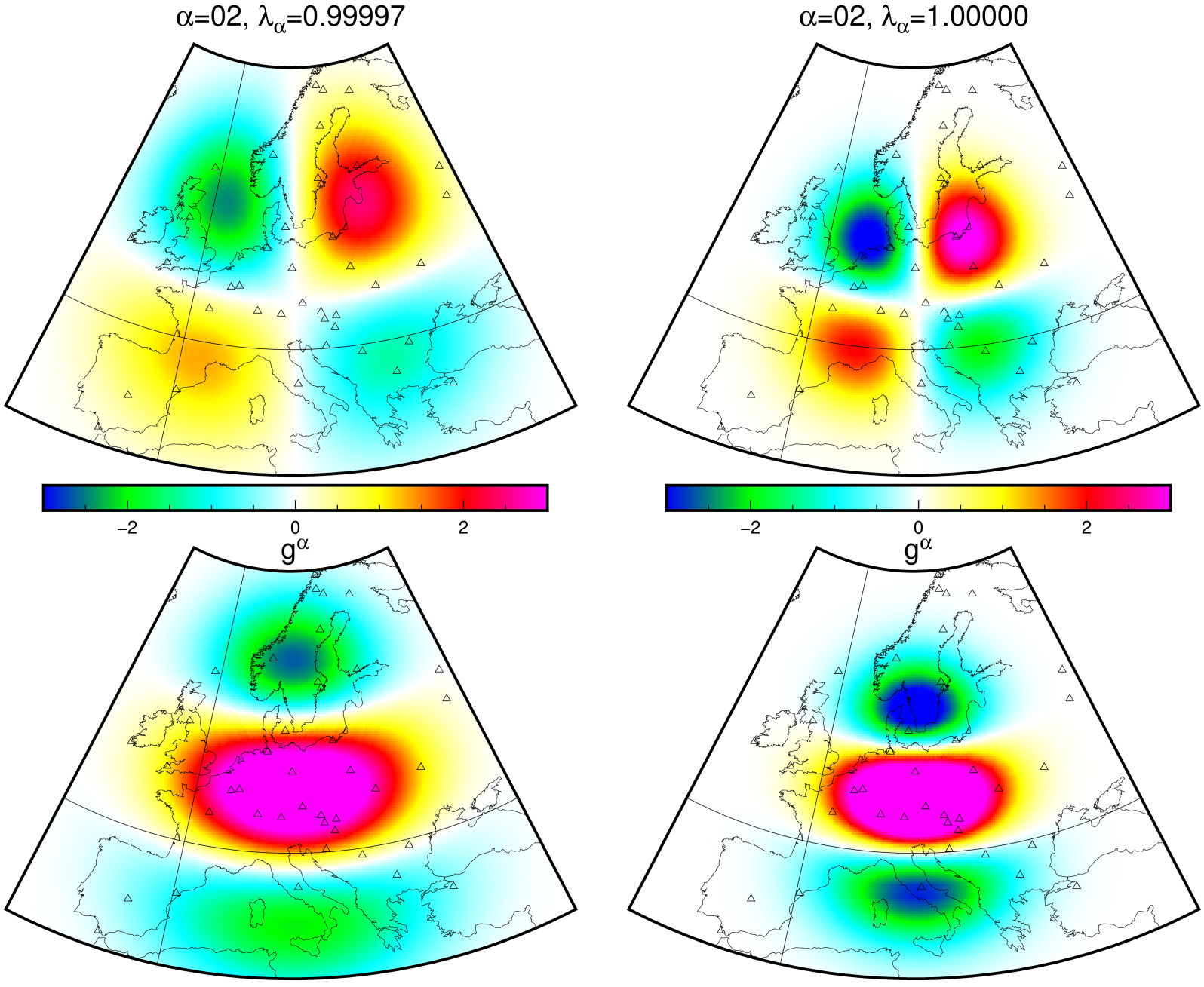


Figure: Second slepian for $j^{\mathrm{s}}_{\max} = 30$ and 60.

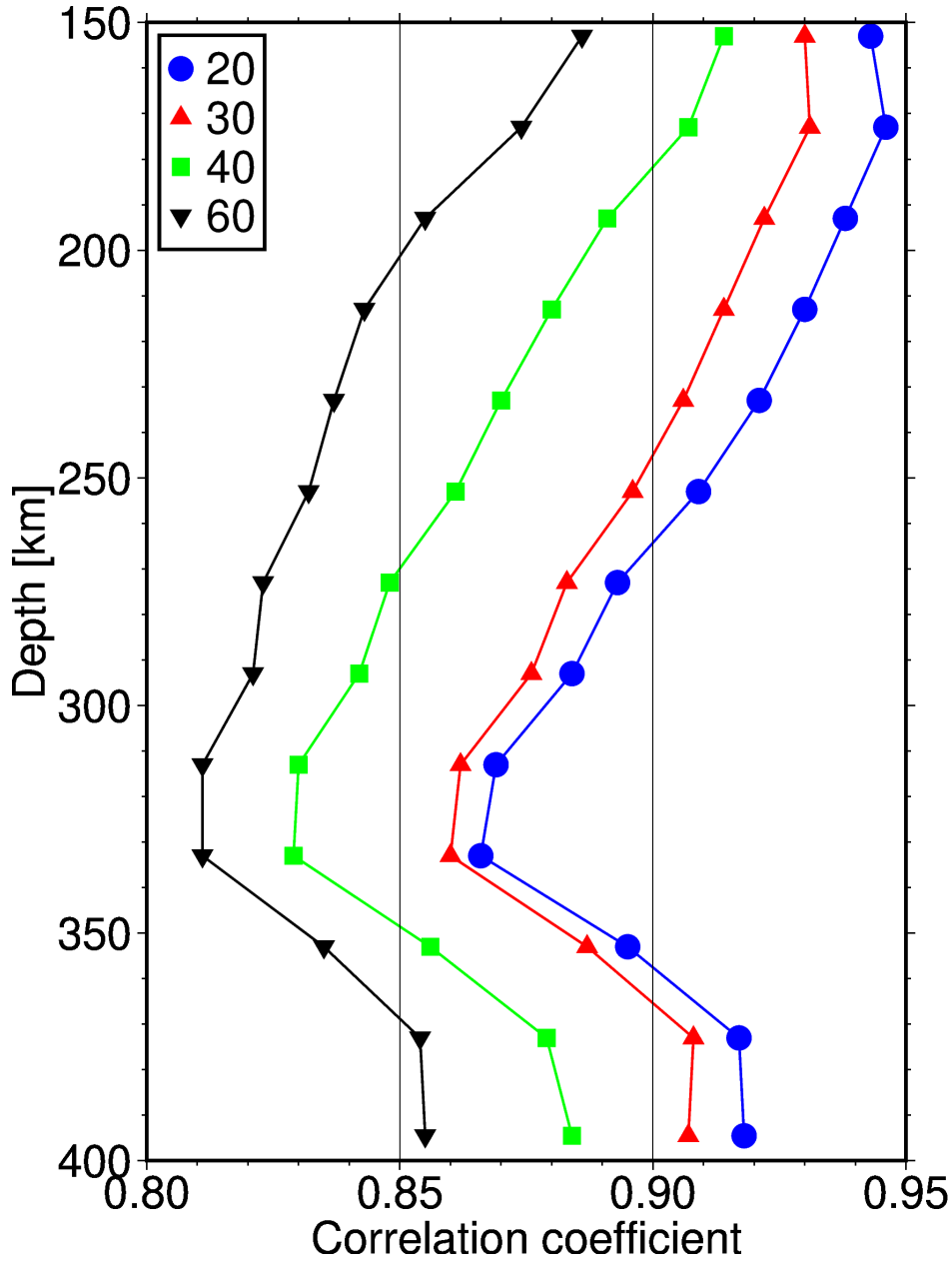


Figure: Depth profiles of correlation coefficients for $T = 24$ h, effect of slepian base.

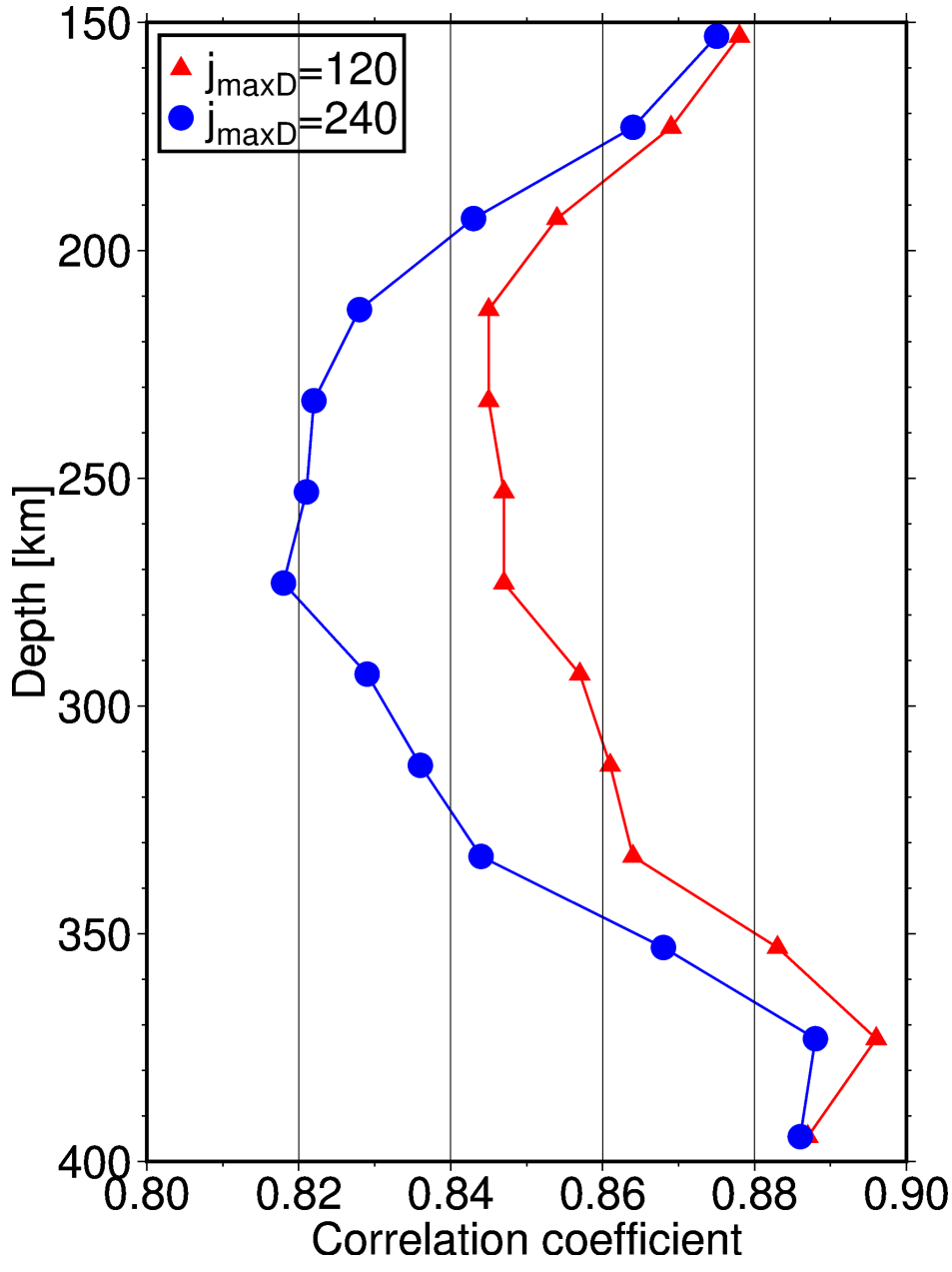


Figure: Depth profiles of correlation coefficients for $T = 24$ h, effect of resolution.

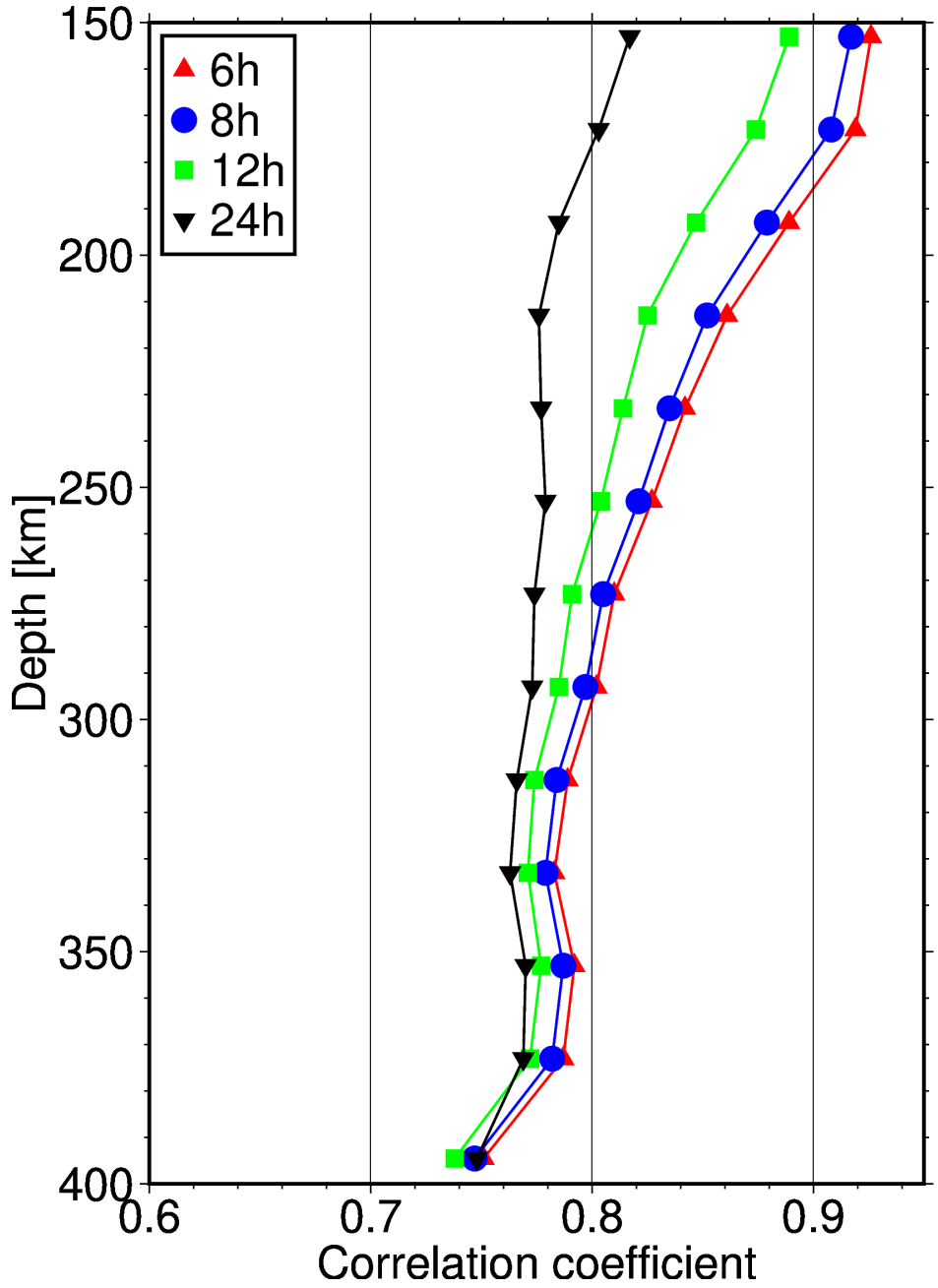


Figure: Depth profiles of correlation coefficients for differnt periods, effect of 5% random perturbations.

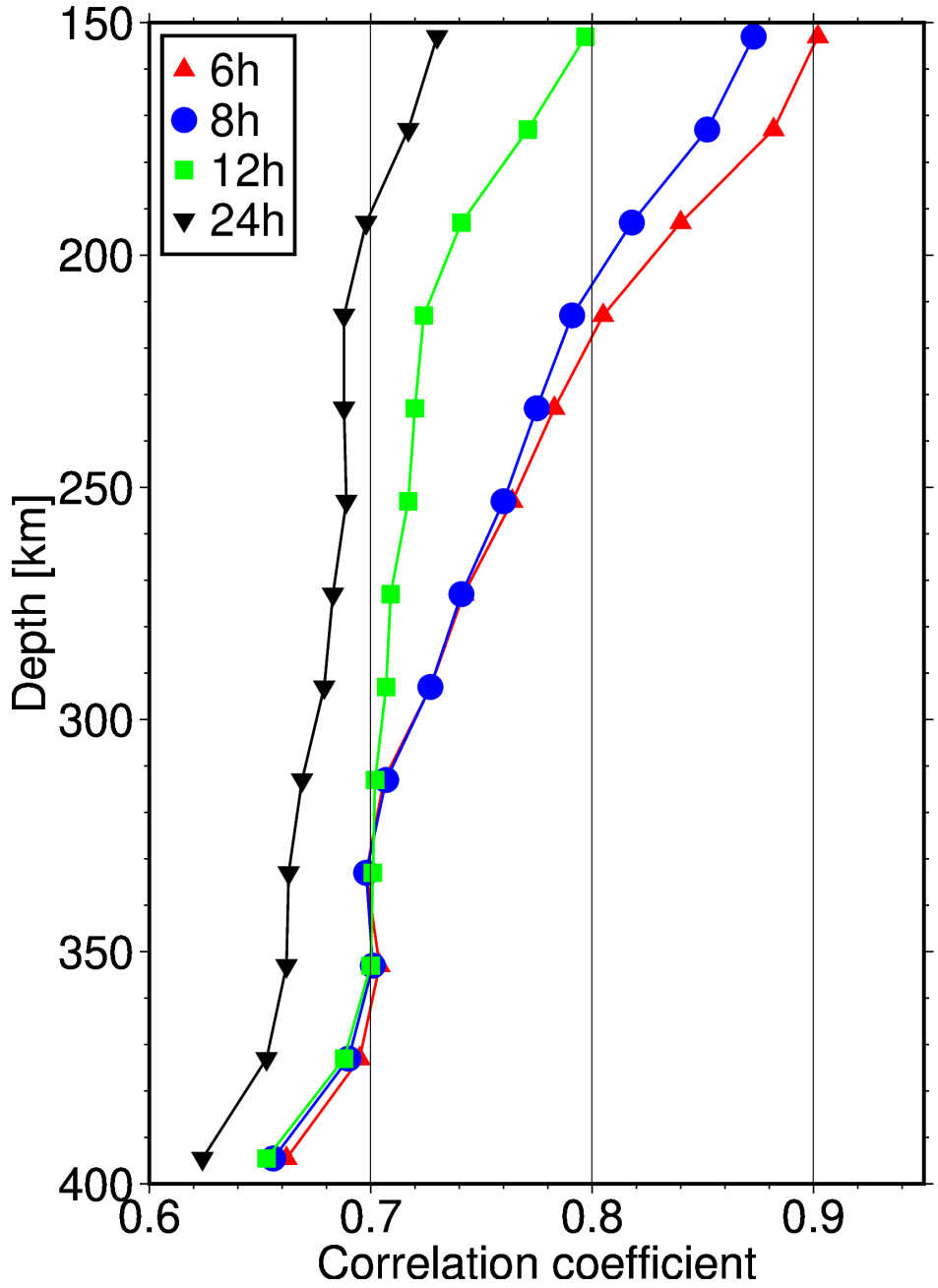


Figure: Depth profiles of correlation coefficients for differnt periods, effect of 10% random perturbations.

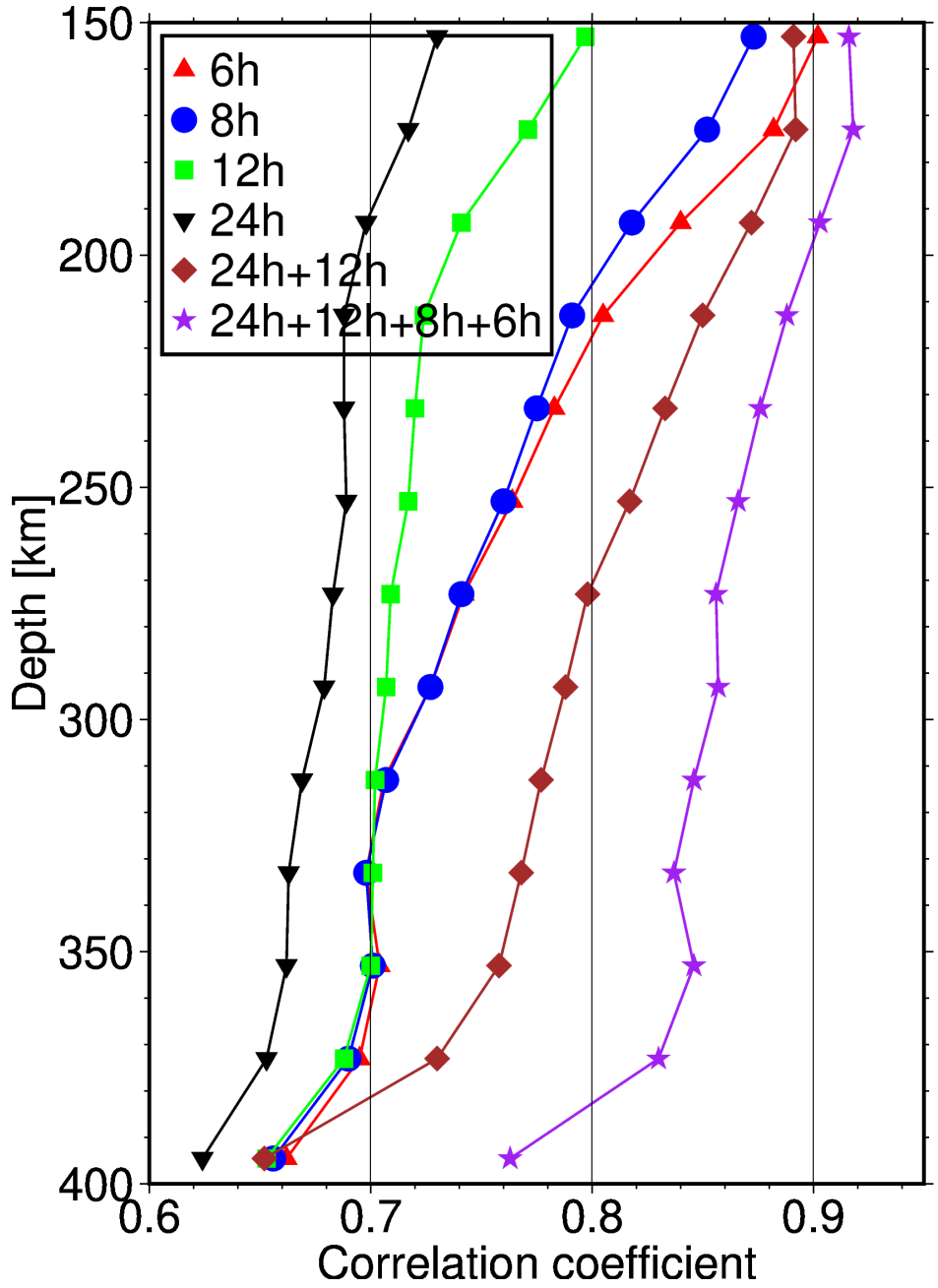


Figure: Depth profiles of correlation coefficients for differnt periods, effect of 10% random perturbations.

Current section

1 Introduction

2 Forward modelling

3 Inverse modelling

4 Synthetic tests

5 3-D inversion of real data

Inversion of real data

- hourly data, 1997–2016
- 42 observatories

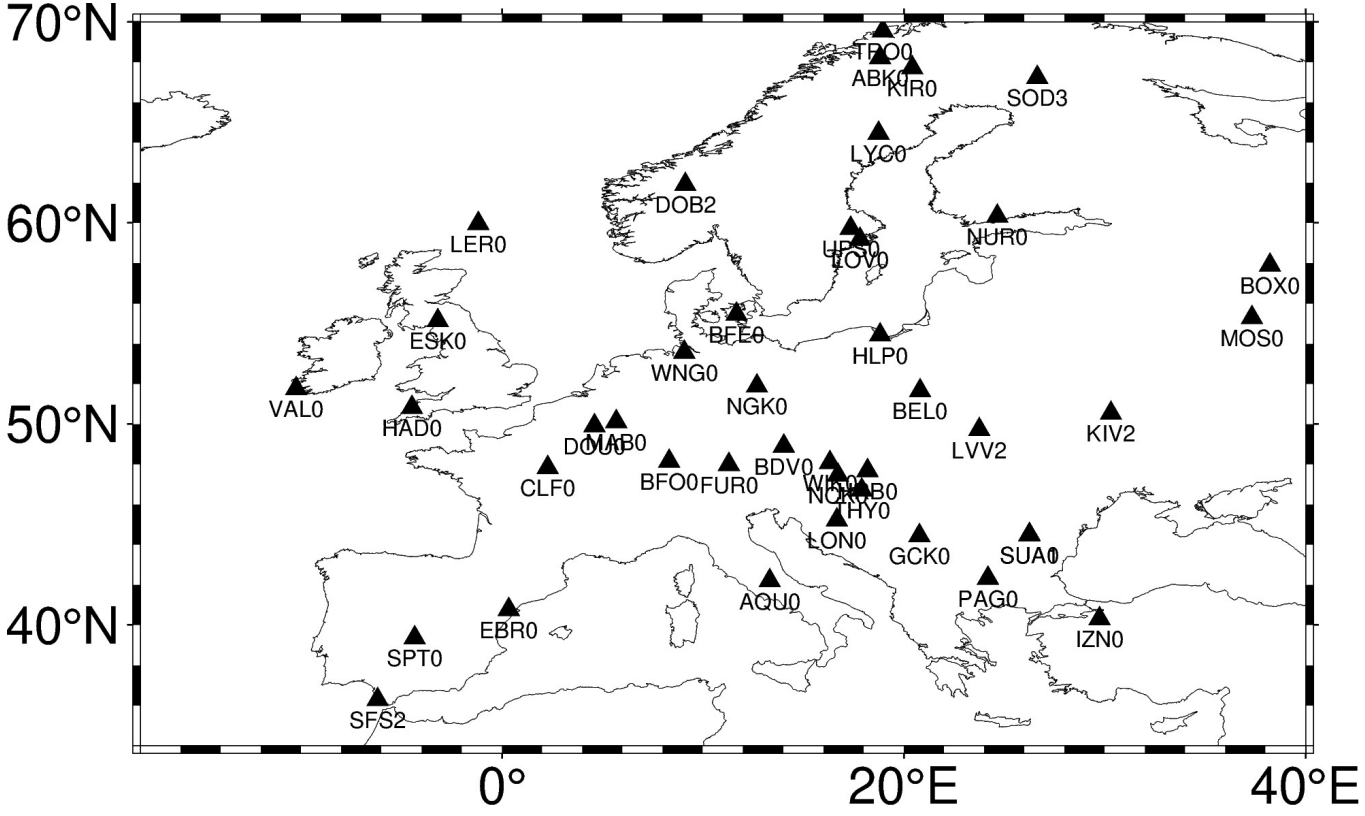


Figure: Available observatories.

- 4 periods (24 h, 12 h, 8 h, 6 h)

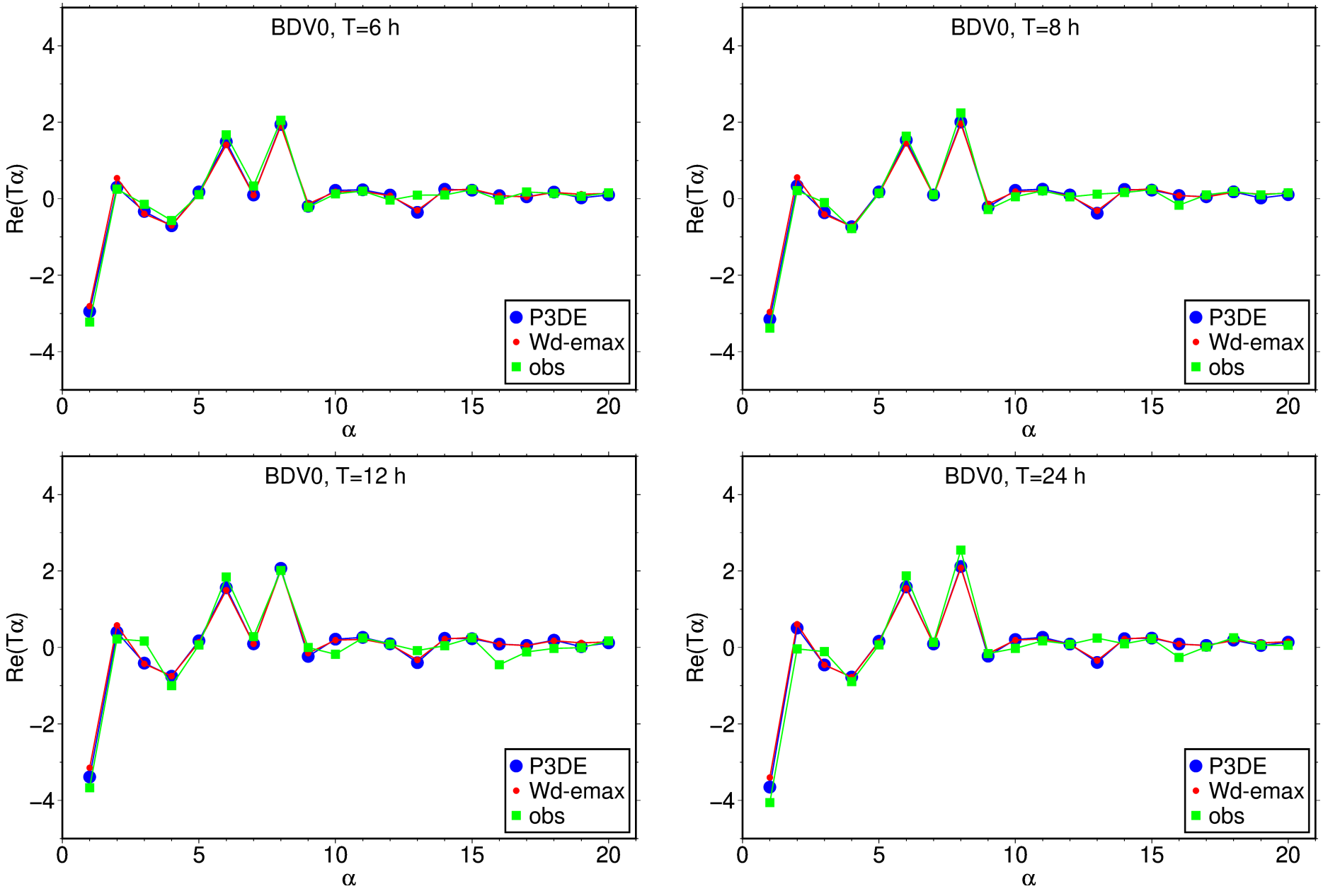


Figure: Effect of period on the real parts of TF.

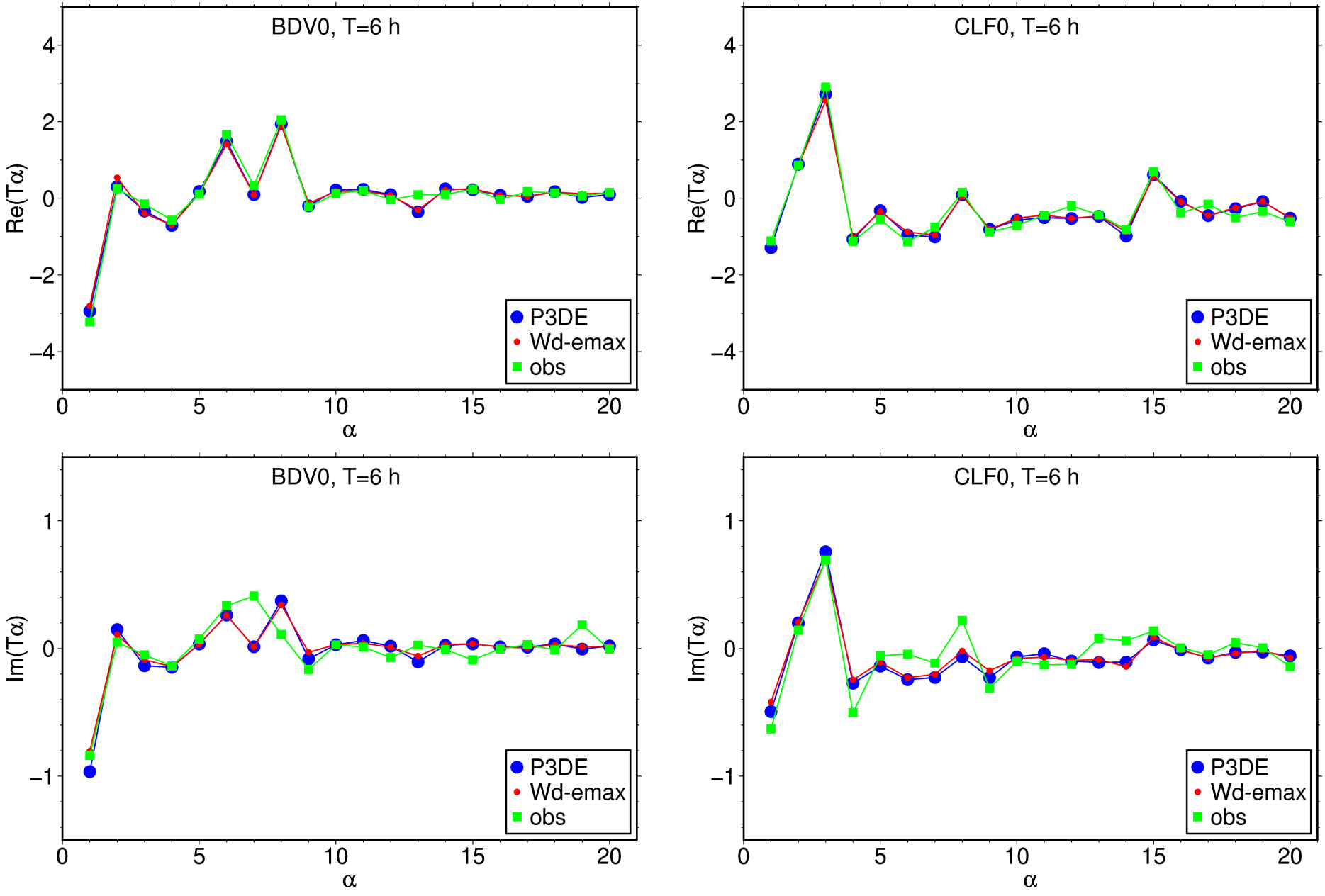


Figure: Real and imaginary parts of $T = 6$ h transfer functions for all slepians at the chosen observatories.

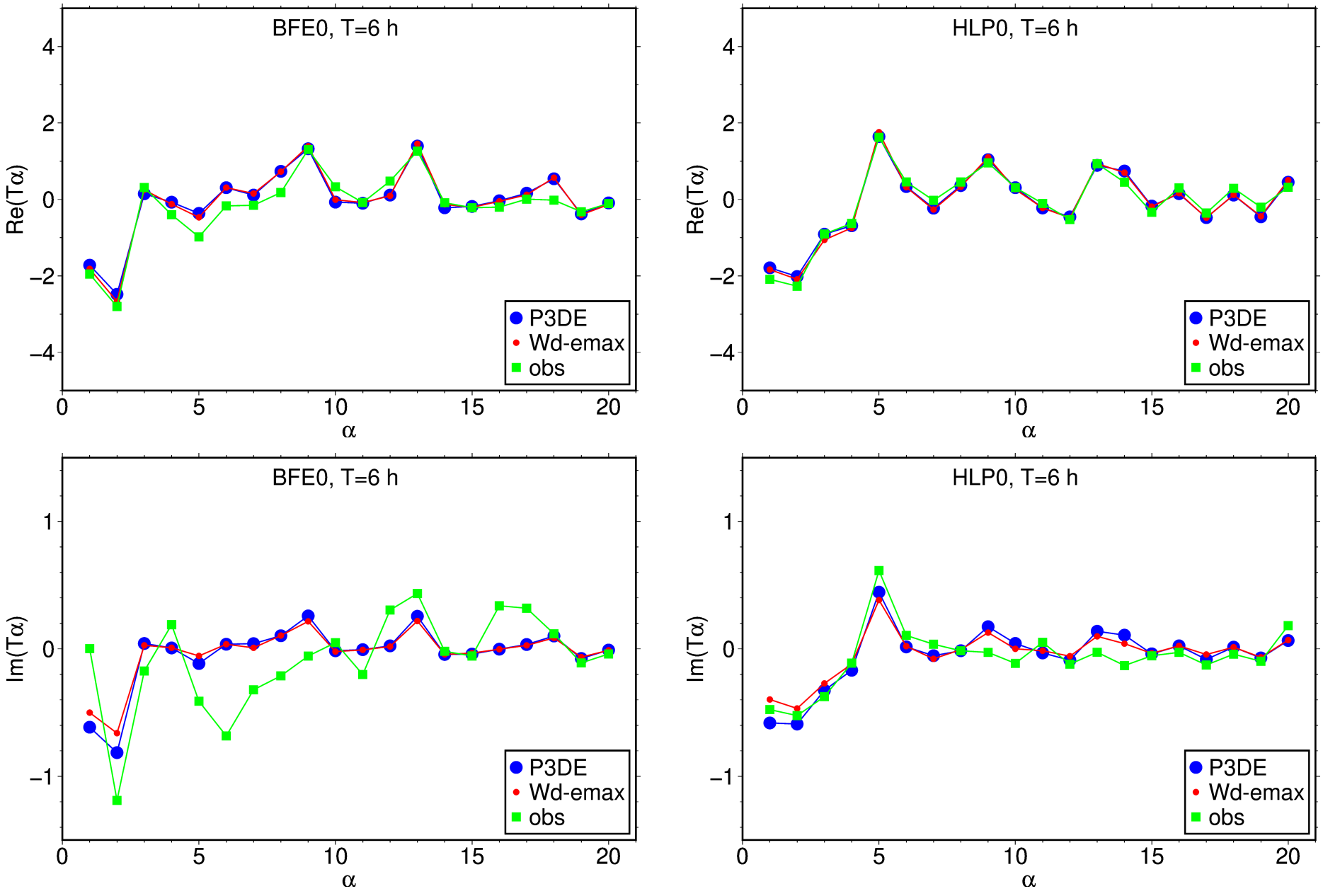


Figure: Real and imaginary parts of $T = 6$ h transfer functions for all slepians at the chosen observatories.

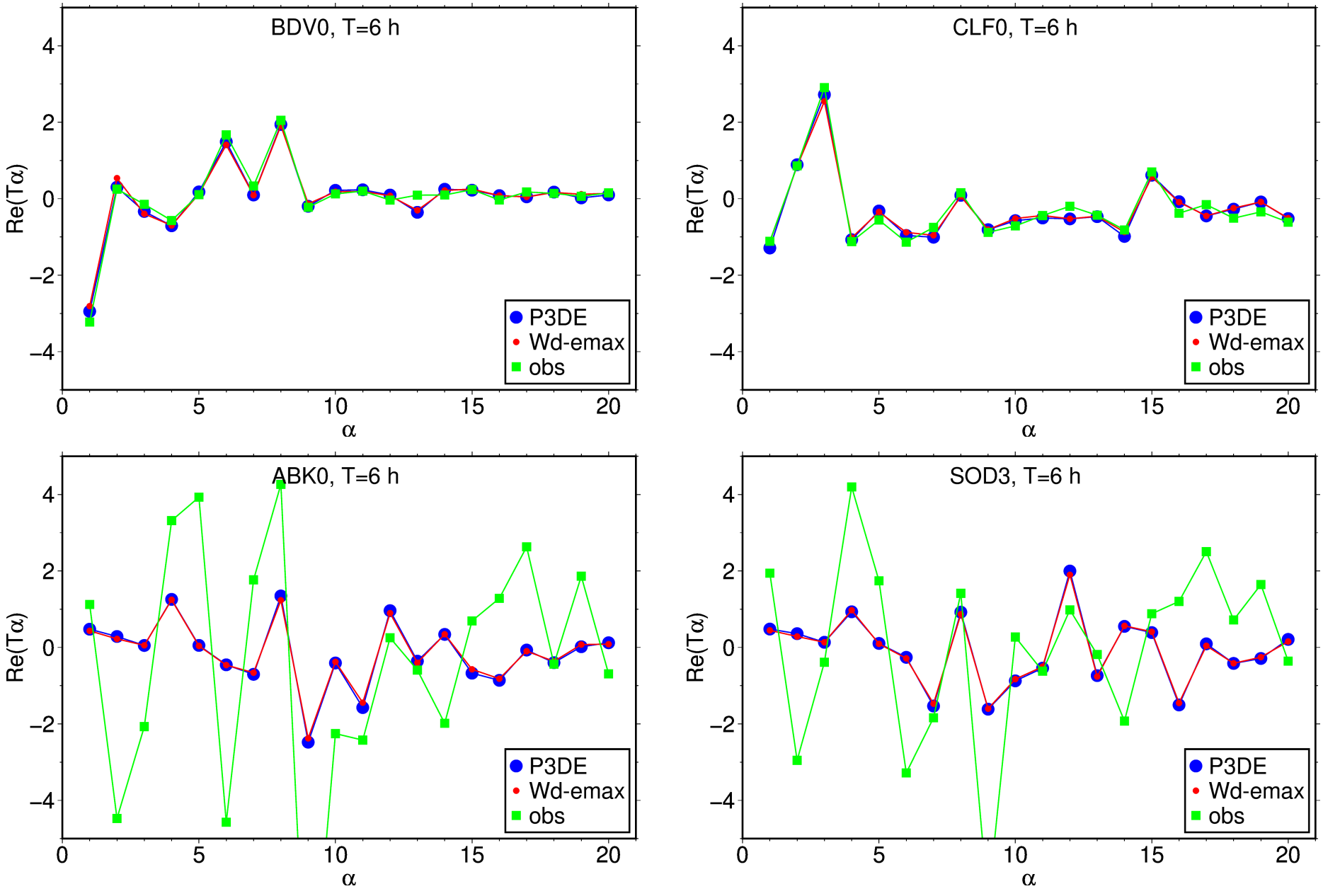


Figure: Agreement and disagreement of TFs.

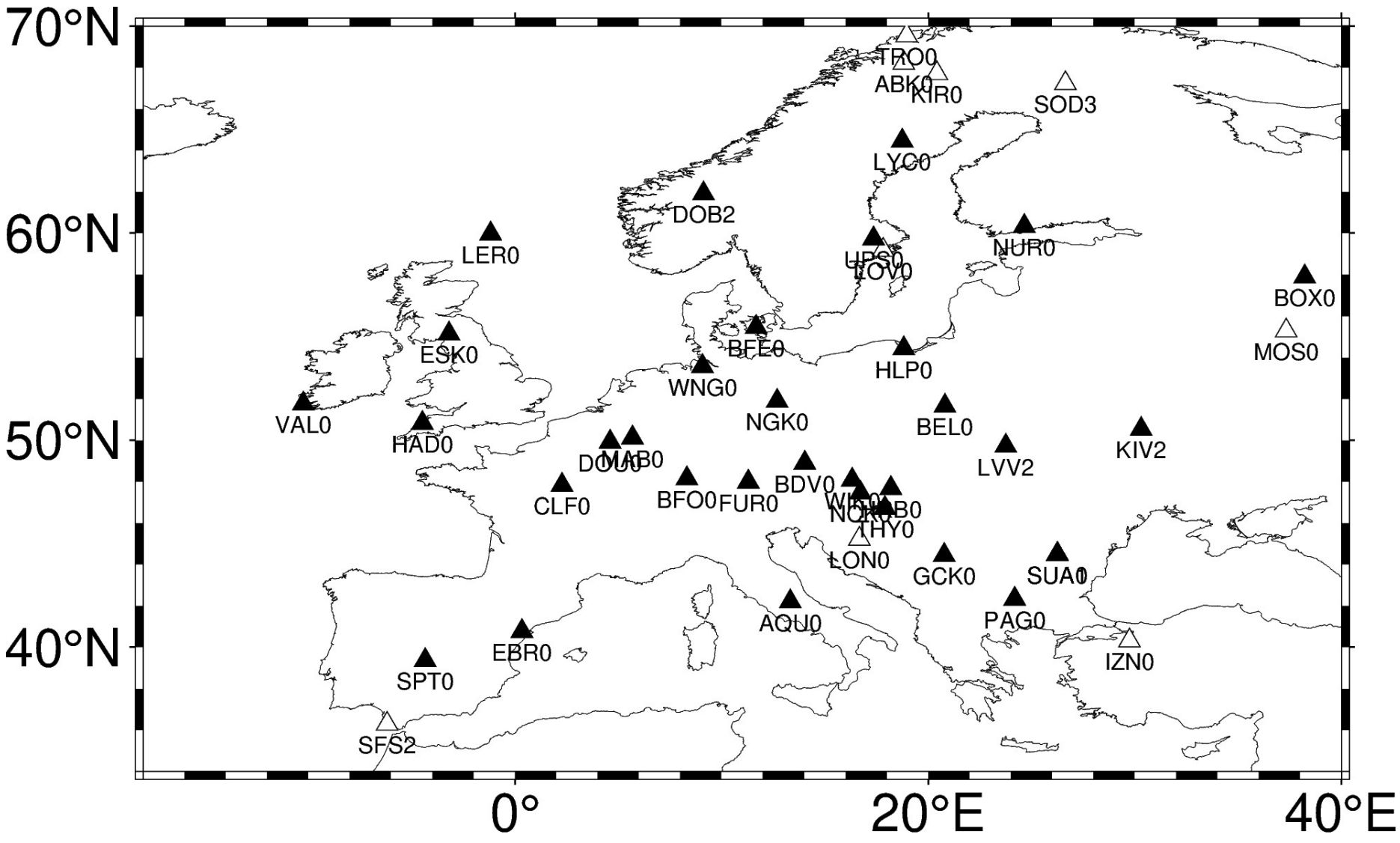


Figure: Available observatories.

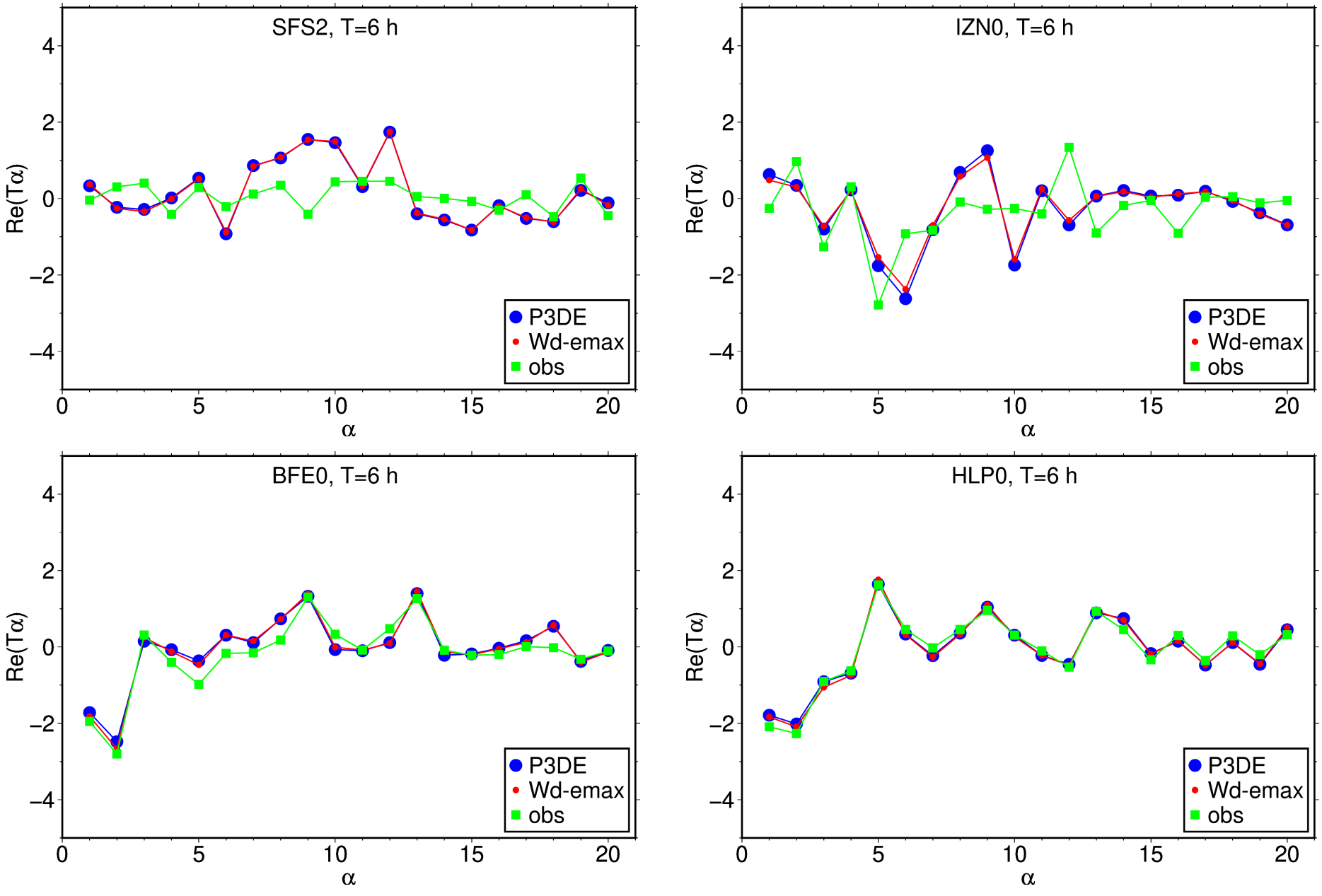


Figure: Effect of uncorrected tidal signal?

Inversion of real data

- 32 observatories
- 4 periods
- $N_s = 3$

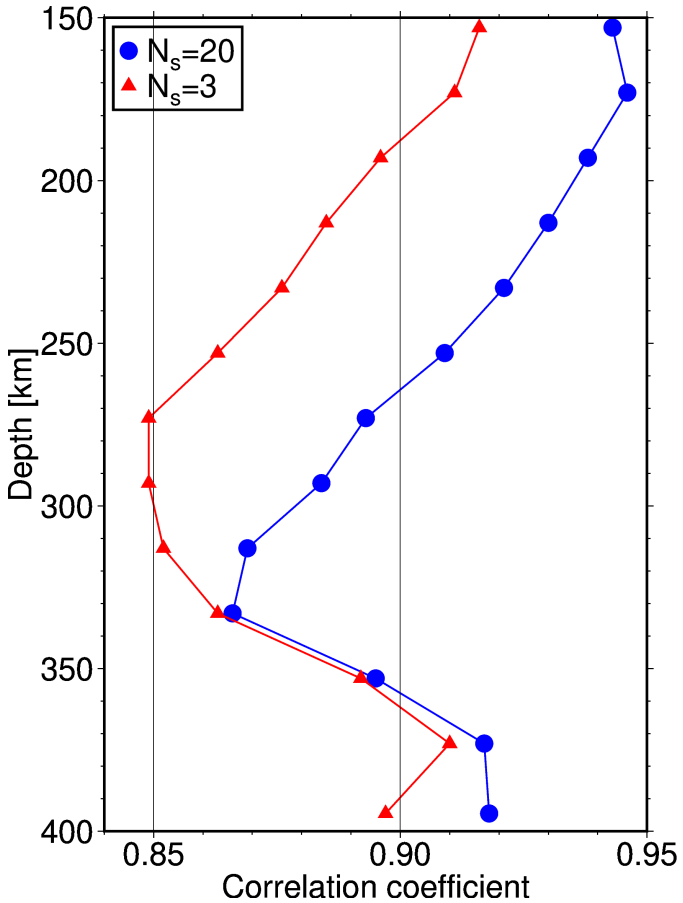
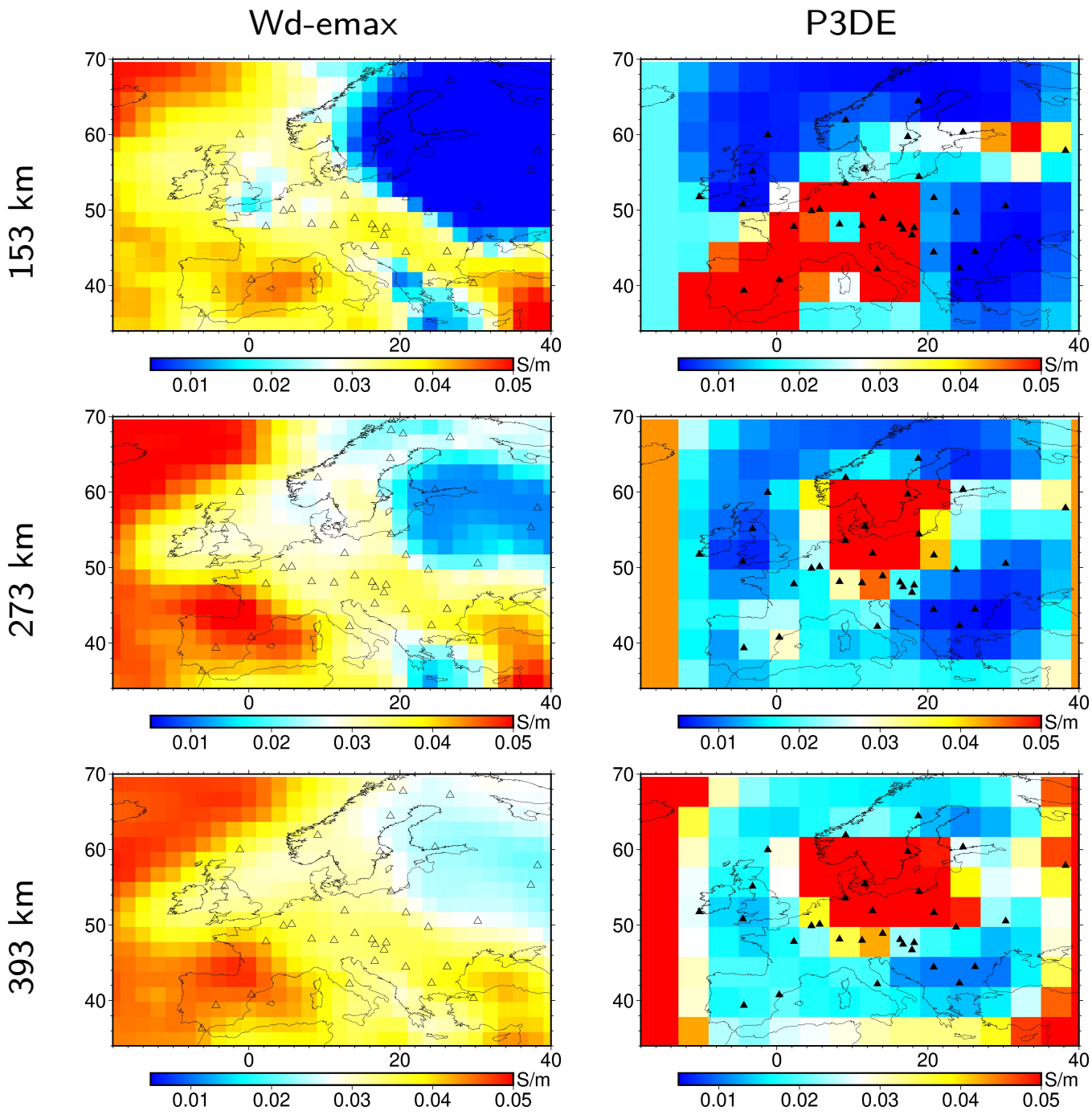
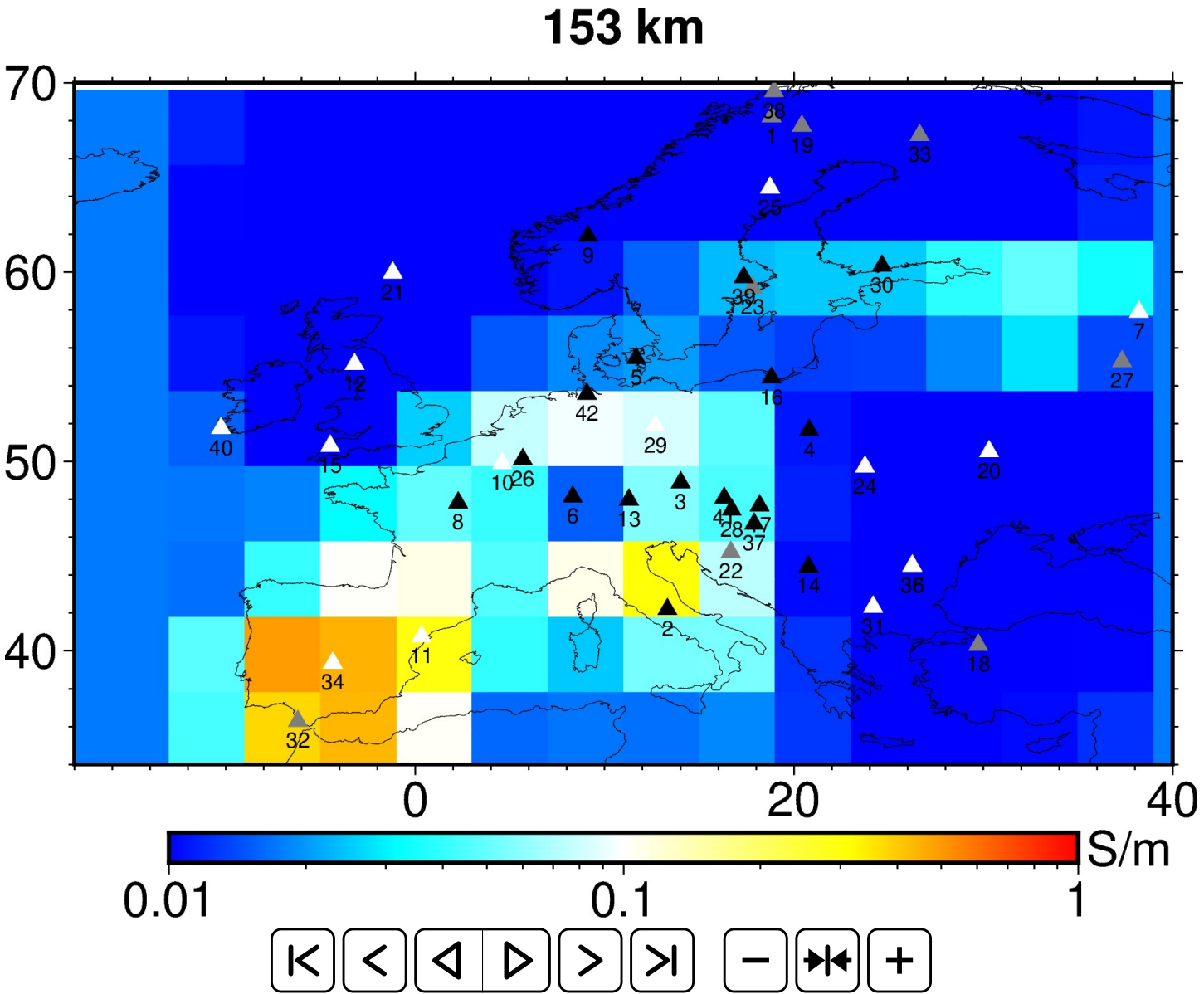


Figure: Depth profiles of correlation coefficients for $T = 24$ h, effect of the number of slepians.


Wd-emax
P3DE
153 km
273 km
393 km
70
60
50
40
0
20
40
S/m
0.01
0.02
0.03
0.04
0.05

Conductivity model P3DE



Is P3DE better than Wd-emax?

Model	**Data misfit**
1-D Wd-emax	0.643
3-D Wd-emax	0.626
P3DE	0.553

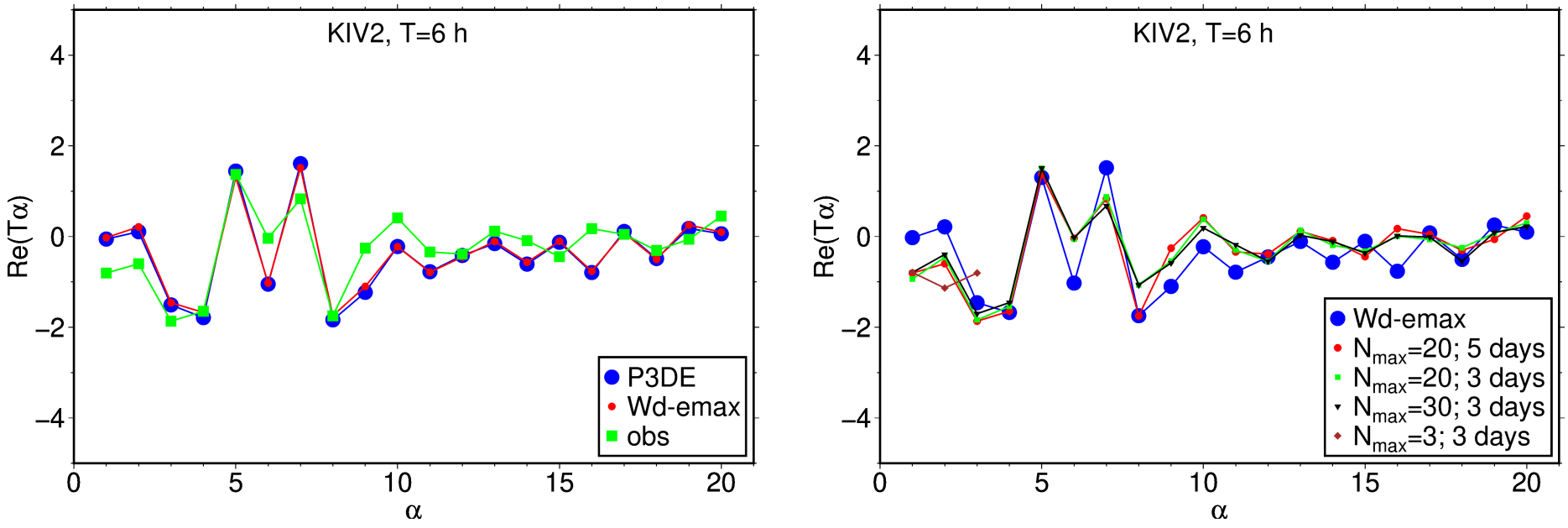


Figure: Real parts of $T = 6$ h KIV2 transfer functions for all slepians.

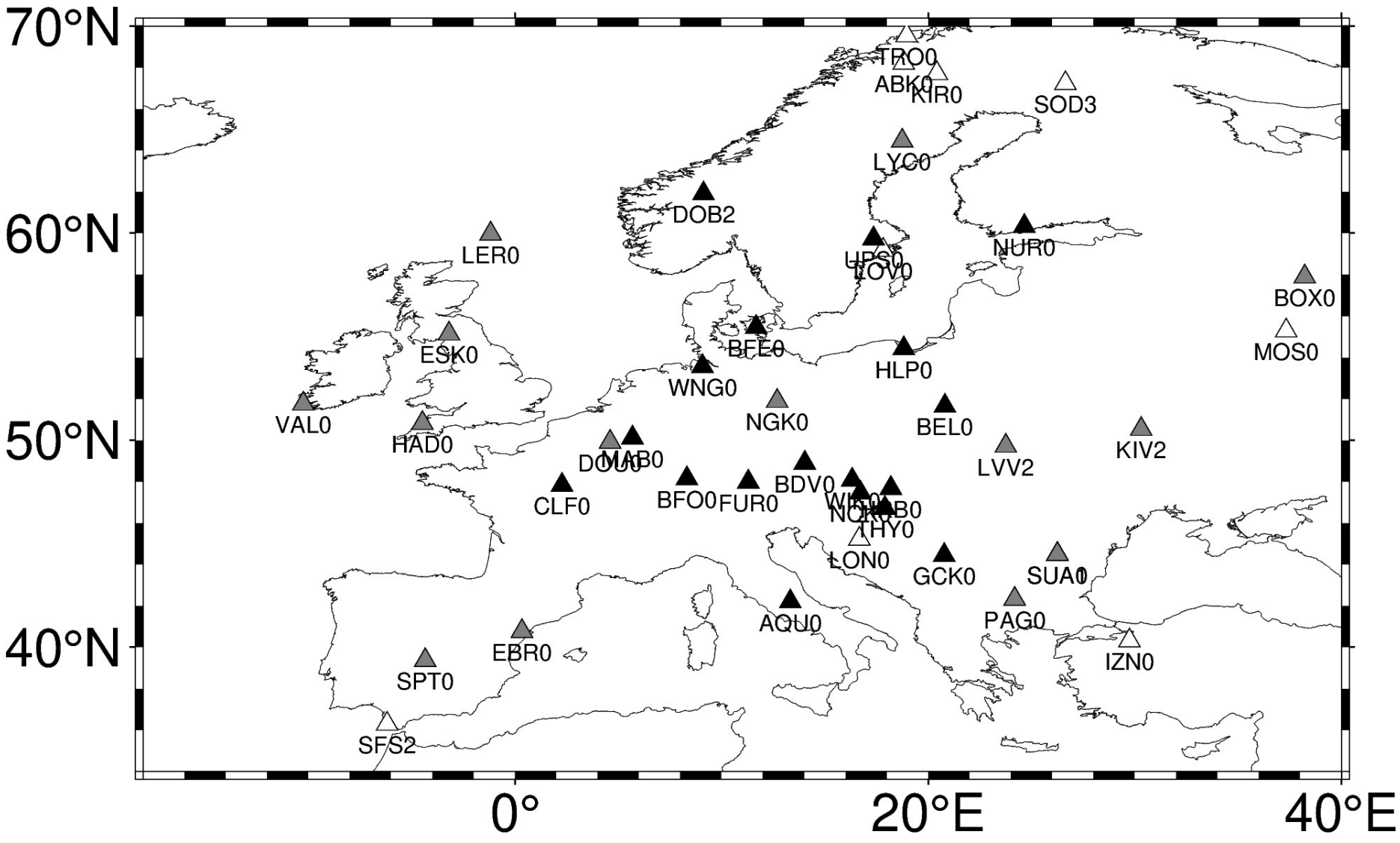


Figure: Available observatories.

Summary

- synthetic data
  - recovered model is in a good agreement with the target model even in the presence of noise
  - 150-400 km $\Rightarrow$ shorter periods outperform longer periods
  - joint inversion with more periods $\Rightarrow$ conductivity is recovered more accurately
- real data
  - imaginary parts of TFs show higher disagreement
  - usage of high-latitiude data is precluded by the magnetospheric signals
  - data processing needs "tuning"

Outlook

- correct data for TIMF
- derive TFs using “high-quality” observatories?
- restrict the inversion to a smaller region

Everett, M.E., Constable, S., Constable, C.G., 2003. Effects of near-surface conductance on global satellite induction responses. Geophys. J. Int. 153, 277–286.

Fullea, J., Lebedev, S., Martinec, Z., Celli, N.L., 2021. WINTERC-G: Mapping the upper mantle thermochemical heterogeneity from coupled geophysical-petrological inversion of seismic waveforms, heat flow, surface elevation and gravity satellite data. Geophys. J. Int. 226, 146–191. doi:doi:10.1093/gji/ggab094.

Grayver, A., Munch, F., Kuvshinov, A., Khan, A., Sabaka, T., Tøffner-Clausen, L., 2017. Joint inversion of satellite-detected tidal and magnetospheric signals constrains electrical conductivity and water content of the upper mantle and transition zone. Geophys. Res. Lett. 44, 6074–6081.

Grayver, A.V., 2021. Global 3-d electrical conductivity model of the world ocean and marine sediments. Geochemistry, Geophysics, Geosystems 22, e2021GC009950.

Maksimov, M., Velímský, J., 2017. Fast calculations of the gradient and the hessian in the time-domain global electromagnetic induction inverse problem. Geophysical Journal International 210, 270–283.

Martinec, Z., Fullea, J., Velímský, J., Šachl, L., 2021. A new integrated geophysical-petrological global three dimensional model of upper-mantle electrical conductivity validated by the swarm M_2 tidal magnetic field. Geophys. J. Int. .

Press, W.H., Teukolsky, S.A., Vetterling, W.T., Flannery, B.P., 1992. Numerical recipes in Fortran. The art of scientific computing. Cambridge University Press, Cambridge.

Šachl, L., Velímskỳ, J., Fullea, J., Martinec, Z., 2022. Inversion of the satellite observations of the tidally induced magnetic field in terms of 3-d upper-mantle electrical conductivity: method and synthetic tests. GJI 229, 2115–2132.

Tyler, R.H., Boyer, T.P., Minami, T., Zweng, M.M., Reagan, J.R., 2017. Electrical conductivity of the global ocean. Earth Planets Space 69, 156.